Vietnam Journal of Science and Technology ***57*** *(6A) (2019) 107-124*

doi:10.15625/2525-2518/57/6A/14643

FREE VIBRATION OF TAPERED FUNCTIONALLY GRADED CARBON NANOTUBE-REINFORCED COMPOSITE BEAMS USING A HIERARCHICAL BEAM ELEMENT

Trinh Thi Hien*

Institute of Mechanics, VAST, 18 Hoang Quoc Viet, Ha Noi, Viet Nam

*Email: *trinhthihien.k56@hus.edu.vn*

Received: 25 November 2019; Accepted for publication: 13 January 2019

Abstract. Free vibration of tapered functionally graded carbon nanotube-reinforced composite (FG-CNTRC) beams is investigated. The beams with four types of carbon nanotube distribution in the thickness, namely the uniform (UD-CNT), X-type (FGX-CNT), A-type (FGA-CNT) and O-type (FGO-CNT), are assumed to be linearly tapered in longitudinal direction by three different taper cases. Based on the first-order shear deformation theory, equations of motion with variable coefficients are derived from Hamilton's principle. Using hierarchical functions to interpolate the displacement field, a two-node beam element with nine degrees of freedom is formulated and employed to compute frequencies of the beams. The accuracy of the derived formulation is confirmed by comparing frequencies obtained in the present work with the published data. The effects of the total CNT volume fraction, CNT distribution type, taper cases, taper ratio, aspect ratio, boundary conditions, etc., on the vibration characteristics of the beams are examined and discussed.

Keywords: Tapered FG-CNTRC beam, first-order shear deformation theory, hierarchical interpolation, beam element, free vibration

Classification numbers: 2.9.4, 5.4.2, 5.4.3.

1. INTRODUCTION

The remarkable mechanical properties of carbon nanotubes (CNTs) such as extremely high elastic modulus and low density make them an excellent material for reinforcement of advanced composites. Experimental and theoretical results show that CNTs are one of the strongest materials known to humans [1, 2]. It has been shown that CNT reinforced composites have better structural functionality than convention al structural elements in terms of high strength-weight ratio, high stiffness-weight ratio, ductility and damping mechanisms [3, 4]. The research confirms that the existence of CNTs in the matrix can induce the frictional sliding damping mechanism, which increases the energy dissipation and suppress the vibration of the composite [5, 6], meanwhile, introduction of CNTs into some thermoplastics can enhance stiffness without sacrificing ductility [7]. The microcracks of structural components usually start from surface defects, which would penetrate through the thickness direction, and then open an oxygen/chemistry path to the internal portion of the structure. As a result, degradation of

structure occurs and causes premature failure. It is anticipated that by using the functionally graded carbon nanotube distribution, the surface of the structure can be armored by a relatively high fraction of CNTs, which can be used to prevent the microcracks from taken place, and a medium fraction of CNTs can provide certain stiffness and strength enhancement.

Some recent researches on mechanical behavior of functionally graded carbon nanotube reinforced composite (FG-CNTRC) beams, the structure considered in the present work, can be mentioned herewith. Ke *et al*. [8] studied nonlinear free vibration of FG-CNTRC Timoshenko beams using the Ritz method and direct iterative technique. They found that both linear and nonlinear frequencies of nanotube composite beams with symmetrical distribution of CNTs are higher than those of beams with uniform or unsymmetrical distribution of CNTs. Using the generalized differential quadrature method, Yas and Samadi [9] investigated free vibration and buckling of FG-CNTRC Timoshenko beams resting on an elastic foundation. It has been shown by the authors that the fundamental frequency and critical load of the beams with X-type distribution of CNTs are higher than that of the beam with the other types of CNT distributions. Large amplitude vibration, nonlinear bending and thermal post-buckling of FGCNTRC beams on elastic foundation under different thermal conditions were investigated by Shen and Xiang [10]. It has been shown by the authors that a CNTRC beam with an intermediate CNT volume fraction does not necessarily have intermediate nonlinear frequencies, buckling temperatures and thermal post-buckling strengths, and also the thermal post-buckling path of unsymmetrical FG-CNTRC beams is no longer the bifurcation type. Adopting a variational approach, Lin and Xiang [11] derived the eigenvalue equations for free vibration analysis of the first- and third-order shear deformation FG-CNTRC beams. The obtained eigenvalue equations were then solved by the p-Ritz method, and a comparison study has been carried out to highlight the differences in vibration frequencies based on the two theories. Based on different shear deformation theories, Wattanasakulpong and Ungbhakorn [12] derived analytical solutions for bending, buckling and vibration problems of FGCRNRC beams resting on a Pasternak elastic foundation. Nejati *et al*. [13] employed the two dimensional elasticity theory and Hamilton's principle to derive stability and motion equations of FG-CNTRC beams, and then used the generalized differential quadrature method to obtain the critical loads and natural frequencies of the beams. Wu *et al*. [14] adopted the von Kármán geometric nonlinearity to study the imperfection sensitivity of post-buckling behavior of a first-order shear deformable FG-CNTRC beam under axial compression. Numerical results obtained by in the work showed that the post-buckling behavior is highly sensitive to the imperfection amplitude, the imperfection mode, and its half-wave number also moderately affect the imperfection sensitivity of the post-buckling response. The same authors, Wu *et al*. [15] considered the imperfection sensitivity of thermal post-buckling behavior of FG-CNTRC beams subjected to in-plane temperature. The differential quadrature method has been used in combination with modified Newton–Raphson technique to trace the thermal post-buckling equilibrium paths. The effects of geometric imperfections on free vibration of FG-CNTRC beams subjected to uniform temperature rise was recently considered by a generic imperfection function [16].

Studies on mechanical behavior of functionally graded (FG) beams with variable cross-section have drawn much attention from researchers in recent years. Shahba *et al*. [17], Gan *et al*. [18] derived stiffness and mass matrices for buckling and vibration analyses of tapered Timoshenko beams with material properties vary in longitudinal direction by a power distribution. Nguyen [19, 20], Nguyen and Gan [21] derived the finite element formulations for large displacement analysis of tapered FGM beams under mechanical loads. Newton-Raphson method was employed in combination with arc-length control technique to compute the large displacement paths of the beams. Recently, Nguyen and Tran [22] studied free vibration of

tapered FGM beams using a finite element formulation. The beams in the work are considered to be formed from four materials with the properties varying in both the thickness and length directions by power graduation laws.

In this article, the free vibration of tapered CNT-RC beams is studied by the finite element method. Four types of carbon nanotube distribution in the thickness direction, namely the uniform distribution (UD-CNT), X-type distribution (FGX-CNT), A-type distribution (FGA-CNT) and O-type distribution (FGO-CNT), are considered. A finite element formulation based on Timoshenko beam theory is derived by using hierarchical functions to interpolate the displacement field is formulated and employed in the analysis. The accuracy of the derived element is confirmed by comparing the frequencies obtained in the present work with the published data. The influence of various factors, including taper cases of the beam, taper ratio, CNT distribution type, total CNT volume fraction, beam aspect ratio and boundary conditions on the natural frequencies of the beams are examined in detail and discussed.

2. TAPERED FG-CNTRC BEAM

A tapered FG-CNTRC beam with length L, rectangular cross-section (b x h) in a Cartesian coordinate system (x, y, z) as depicted in Fig. 1 is considered. In the figure, the x-axis is chosen on the mid-plane and the z-axis directs along the thickness direction. The beam is assumed to be longitudinally tapered in three following taper cases

$$\begin{aligned}
&\text{Case A:} \quad A(x) = A_0\left(1-\alpha\frac{x}{L}\right), \quad I(x) = I_0\left(1-\alpha\frac{x}{L}\right)\\
&\text{Case B:} \quad A(x) = A_0\left(1-\alpha\frac{x}{L}\right), \quad I(x) = I_0\left(1-\alpha\frac{x}{L}\right)^3\\
&\text{Case C:} \quad A(x) = A_0\left(1-\alpha\frac{x}{L}\right)^2, \quad I(x) = I_0\left(1-\alpha\frac{x}{L}\right)^4
\end{aligned} \tag{1}$$

where $A(x)$ and $I(x)$ are, respectively, the area and inertia moment of cross section; A_0 and I_0 respectively denote the cross-sectional area and moment of inertia of cross-section at the left end (at $x = 0$); $0 \le \alpha < 1$ is the taper ratio. The beam becomes uniform when $\alpha = 0$.

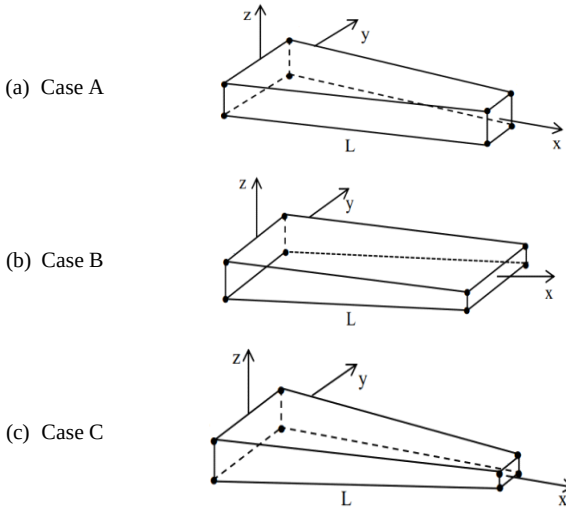

Figure 1. Geometry of FG-CNTRC beams with three taper cases.

Four types of CNT distribution in the beam cross section, namely the uniformly distributed (UD-CNT), functionally graded type A (FGA-CNT), functionally graded type X (FGX-CNT) and functionally graded type O (FGO-CNT), as depicted in Fig. 2 are considered. The mathematical functions used for describing the distribution of material constituents are as follows [9]

UD-CNT: $$V_{CNT}(z) = V_{tcnt}, \quad \left(-\frac{h}{2} \le z \le \frac{h}{2}\right). \tag{2}$$

FGA-CNT: $$V_{CNT}(z) = \left(1 - \frac{2z}{h}\right) V_{tcnt}, \quad \left(-\frac{h}{2} \le z \le \frac{h}{2}\right) \tag{3}$$

FGX-CNT: $$V_{CNT}(z) = \begin{cases} \dfrac{4z}{h} V_{tcnt} & \left(0 \le z \le \dfrac{h}{2}\right) \\ -\dfrac{4z}{h} V_{tcnt} & \left(-\dfrac{h}{2} \le z < 0\right) \end{cases} \tag{4}$$

FGO-CNT: $$V_{CNT}(z) = \begin{cases} \left(2 - \dfrac{4z}{h}\right) V_{tcnt} & \left(0 \le z \le \dfrac{h}{2}\right) \\ \left(2 + \dfrac{4z}{h}\right) V_{tcnt} & \left(-\dfrac{h}{2} \le z < 0\right) \end{cases} \tag{5}$$

where V_{tcnt} is the total CNT volume fraction, and it is assumed to be the same for the four types of the CNT distribution.

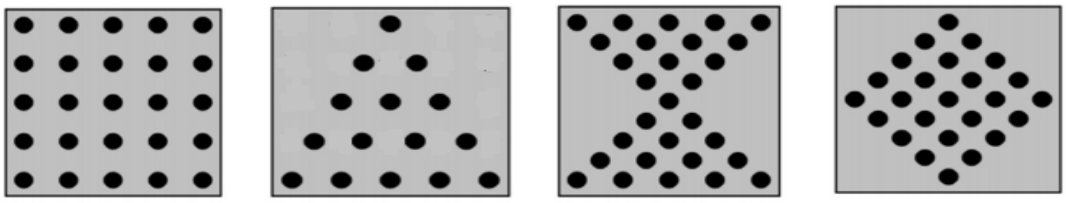

(a) UD-CNT (b) FGA-CNT (c) FGX-CNT (d) FGO-CNT

Figure 2. Cross-sections of four different types of FG-CNTRC beam.

The effective material properties of the FG-CNTRC beam can be estimated using the rule of mixture. The expressions of the effective Young's modulus, shear modulus, Poisson's ratios and mass densities of the beam are of the following forms [11]

$$\begin{aligned} E_{11}(z) &= \eta_1 V_{CNT}(z) \mathrm{E}_{11}^{cnt} + V_m(z) E^m, \\ \frac{\eta_2}{E_{22}(z)} &= \frac{V_{CNT}(z)}{E_{22}^{cnt}} + \frac{V_m(z)}{E^m}, \\ \frac{\eta_3}{G_{12}(z)} &= \frac{V_{CNT}(z)}{G_{12}^{cnt}} + \frac{V_m(z)}{G^m}, \\ \nu_{12}(z) &= V_{CNT}(z) \nu_{12}^{cnt} + V_m(z) \nu^m, \end{aligned} \tag{6}$$

$$\nu_{21}(z)=\frac{\nu_{12}(z)}{E_{11}(z)}\mathrm{E}_{22}(z),$$
$$\rho(z)=V_{CNT}(z)\rho^{cnt}+V_m(z)\rho^m,$$
$$V_m(z)=1-V_{CNT}(z).$$

where $E_{11}^{cnt}, E_{22}^{cnt}, G_{12}^{cnt}, E^m, G^m$ are Young's modulus and shear modulus of CNT and matrix, respectively; η_1,η_2,η_3 are efficiency parameters; $V_{CNT}(z)$ and $V_m(z)$ are, respectively, the volume fractions of CNT and matrix; ν_{12}^{cnt} and ν^m are Poisson's ratios; ρ^{cnt} and ρ^m are mass densities of CNT and matrix, respectively

3. MATHEMATICAL MODEL

Based on the firs-order shear deformation theory, the axial displacement $u(x,z,t)$ and transverse displacement $w(x,z,t)$ at any point of the beam are of the forms

$$u(x,z,t)=u_0(x,t)-z\theta(x,t)$$
$$w(x,z,t)=w_0(x,t) \tag{7}$$

where z is the distance from the mid-plane to the considering point; $u_0(x,t)$ and $w_0(x,t)$ are, respectively, axial and transverse displacements of the corresponding point on the mid-plane, and $\theta(x,t)$ is the rotation of the cross section.

The axial strain (ε_{xx}) and the shear strain (γ_{xz}) are resulted from Eq. (7) are

$$\varepsilon_{xx}=u_{0,x}-z\theta_{,x},\ \gamma_{xz}=w_{0,x}-\theta \tag{8}$$

where and hereafter, a subscript comma is used to indicate the derivative of the variable with respect to the spatial coordinate x.

Assuming elastic behavior, the constitutive equation of the FG-CNTRC beam can be written in the form

$$\begin{Bmatrix}\sigma_{xx}\\ \tau_{xz}\end{Bmatrix}=\begin{bmatrix}E(z) & 0\\ 0 & G(z)\end{bmatrix}\begin{Bmatrix}\varepsilon_{xx}\\ \gamma_{xz}\end{Bmatrix} \tag{9}$$

where σ_{xx} and τ_{xz} are, respectively, the axial and shear stresses; $E(z)$ and $G(z)$ are the effective Young's modulus and shear modulus, respectively. These effective moduli for the FG-CNTRC beam are given by [11]

$$E(z)=\frac{E_{11}(z)}{1-\nu_{12}(z)\nu_{21}(z)},$$
$$G(z)=G_{12}(z) \tag{10}$$

The elastic strain energy for a beam (U) is of the form

$$U=\frac{1}{2}\int_V\left(\sigma_{xx}\varepsilon_{xx}+\psi\tau_{xz}\gamma_{xz}\right)dV$$
$$=\frac{1}{2}\int_0^L\left[A_{11}u_{0,x}^2-2A_{12}u_{0,x}\theta_{,x}+A_{22}\theta_{,x}^2+\psi A_{33}\left(w_{0,x}-\theta\right)^2\right]dx \tag{11}$$

where ψ is the shear correction factor, chosen by 5/6 for the beams with rectangular cross-section considered herein; A_{11}, A_{12}, A_{22} and A_{33} are, respectively, the axial, axial-bending coupling, bending and shear rigidities, defined as

$$(A_{11}, A_{12}, A_{22}) = \int_{A(x)} E(z)(1, z, z^2)dA,\ A_{33} = \int_{A(x)} G(z)dA \tag{12}$$

The kinetic energy for the beam ($\mathcal{T}$) resulted from Eq. (7) is of the form

$$\begin{aligned} \mathcal{T} &= \frac{1}{2}\int_V \rho(z)(\dot{u}^2 + \dot{w}^2)dV \\ &= \frac{1}{2}\int_0^L [I_{11}(\dot{u}_0^2 + \dot{w}_0^2) - 2I_{12}\dot{u}_0\dot{\theta} + I_{22}\dot{\theta}^2]dx \end{aligned} \tag{13}$$

in which an over dot is used to indicate the differentiation with respect to time variable *t*, and I_{11}, I_{12}, I_{22} are the mass moments, defined as

$$\left(I_{11}, I_{12}, I_{22}\right) = \int_{A(x)} \rho(z)\left(1, z, z^2\right)dA \tag{14}$$

Equations of motion for the tapered FG-CNTRC beam can be obtained by applying Hamilton's principle to Eqs. (11) and (13), and they have the following forms

$$\begin{cases} I_{11}\ddot{u}_0 - I_{12}\ddot{\theta} - \left(A_{11}u_{0,x} - A_{12}\theta_{,x}\right)_{,x} = 0 \\ I_{11}\ddot{w}_0 - \psi\left[A_{33}\left(w_{0,x} - \theta\right)\right]_{,x} = 0 \\ I_{12}\ddot{u}_0 - I_{22}\ddot{\theta} - \left(A_{12}u_{0,x} - A_{22}\theta_{,x}\right)_{,x} + \psi A_{33}\left(w_{0,x} - \theta\right) = 0 \end{cases} \tag{15}$$

Different essential boundary conditions (B.C.) of the beams, namely hinged-hinged (H-H), clamped-hinged (C-H), clamped-clamped (C-C), clamped-free (C-F) are considered herein. These conditions are described through the displacement components as

Clamped (C): $u_0 = w_0 = \theta = 0$

Hinged (H): $u_0 = w_0 = 0$ (16)

Free (F): There is no binding

4. FINITE ELEMENT FORMULATION

The coefficients of the equation of motion (15), as seen from Eqs. (12) and (14), are functions of coordinate x, a closed-form solution for Eq. (15) is hardly obtained. A finite beam element is derived in this section for solving the equation of motion of the tapered FG-CNTRC beam. Consider a two-node beam element of length *l* with the axial displacement u_0, the rotation θ and transverse displacement w_0 are interpolated by using the hierarchical functions as

$$\begin{aligned} u_0 &= N_1u_1 + N_2u_2 \\ \theta &= N_1\theta_1 + N_2\theta_2 + N_3\theta_3 \\ w_0 &= N_1w_1 + N_2w_2 + N_3w_3 + N_4w_4 \end{aligned} \tag{17}$$

where $u_1, u_2, \theta_1, \theta_2, \theta_3, w_1, ..., w_4$ are nine unknown values of the variables. Noting that θ_3, w_3 and w_4 are not values of the variables at the nodes. In Eq. (17), N_1 and N_2 are linear functions, while N_3 and N_4 are, respectively, quadratic and cubic polynomials. The functions N_3 and N_4 can be generated from N_1 and N_2 by adding a higher-order term and choosing a point between the two nodes. By selecting a value at mid-point element for θ, two values at quarter and three-quarter of the element for w, one can obtain the following the hierarchical shape functions [23]

$$N_1 = \frac{1}{2}(1-\xi), \quad N_2 = \frac{1}{2}(1+\xi) \tag{18}$$
$$N_3 = (1-\xi^2), \quad N_4 = \xi(1-\xi^2)$$

with $\xi = 2\frac{x}{l} - 1$ is the natural coordinate. The above four functions in Eq. (18) are illustrated in Fig. 3(a). It is necessary to note that the used of the above hierarchical interpolation can avoid to redetermination of interpolation functions in mesh refinement as in case of the standard polynomials [24]. In addition, the hierarchical functions can also prevent the formulated beam element from the shear locking, the problem occurs in the first-order shear deformable beam element using linear interpolation [25].

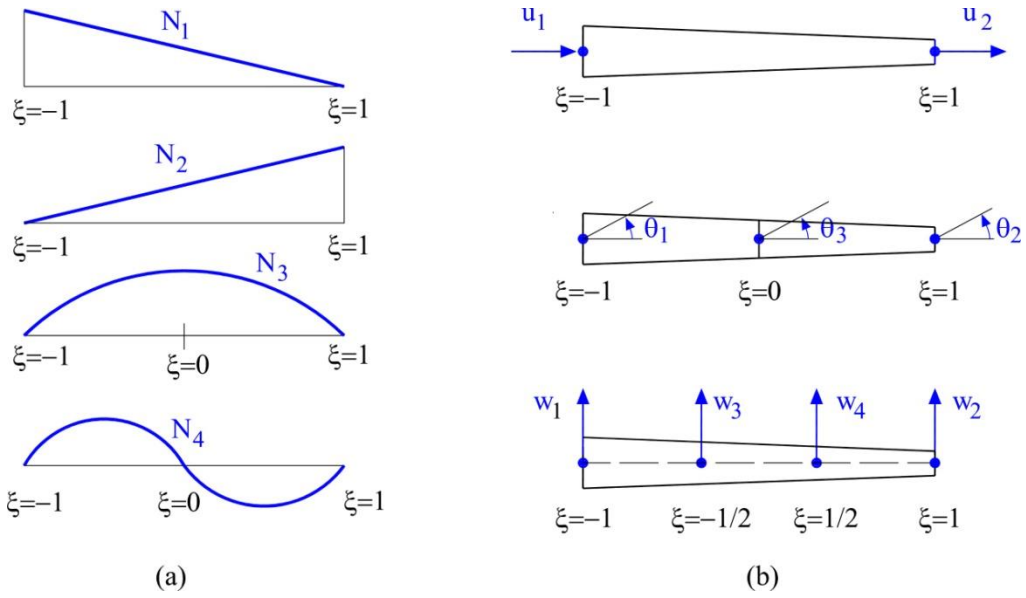

Figure 3. Hierarchical functions (a), and detail of degrees of freedom for the beam element (b).

The element vector of nodal displacements for a generic beam element has nine unknown as follows

$$\mathbf{d} = \{ u_1 \;\; w_1 \;\; \theta_1 \;\; w_3 \;\; \theta_3 \;\; w_4 \;\; u_2 \;\; w_2 \;\; \theta_2 \}^T \tag{19}$$

where u_i, w_i and θ_i (i = 1, 2) are, respectively, the displacements and rotations at the nodes 1 and 2, and w_3 , w_4 , θ_3 are the values of the transverse displacement and rotation between the two nodes. The detail of the degrees of freedom for the present element is depicted in Fig. 3(b).

In a matrix form, one can write the interpolation (17) and (18) as follows

$$u_0 = \mathbf{N}_u \mathbf{d},\ \theta = \mathbf{N}_\theta \mathbf{d},\ w_0 = \mathbf{N}_w \mathbf{d} \tag{20}$$

in which

$$\begin{aligned}
\mathbf{N}_u &= [\,N_1 \ \ 0 \ \ 0 \ \ 0 \ \ 0 \ \ 0 \ \ N_2 \ \ 0 \ \ 0\,] \\
\mathbf{N}_\theta &= [\,0 \ \ 0 \ \ N_1 \ \ 0 \ \ N_3 \ \ 0 \ \ 0 \ \ 0 \ \ N_2\,] \\
\mathbf{N}_w &= [\,0 \ \ N_1 \ \ 0 \ \ N_3 \ \ 0 \ \ N_4 \ \ 0 \ \ \mathrm{N}_2 \ \ 0\,]
\end{aligned}$$

are the matrices of interpolation functions for u_0, θ and w_0, respectively.

Substituting u_0, w_0, θ from (20) into the strain energy expression, Eq. (11), one gets

$$U = \frac{1}{2}\sum_{i=1}^{ne} \mathbf{d}_i^T \mathbf{k}_i \mathbf{d}_i \tag{22}$$

where *ne* is total number of the elements; **k** is stiffness matrix of the element beam. Noting that $(.)_{,x} = \frac{2}{l}(.)_{,\xi}$ and $dx = \frac{l}{2}d\xi$, one can write the element matrix in the following form

$$\begin{aligned}
\mathbf{k} \ = \ & \frac{2}{l}\int_{-1}^{1}\left(\mathbf{N}_{u,\xi}^T A_{11}\mathbf{N}_{u,\xi} - 2\mathbf{N}_{u,\xi}^T A_{12}\mathbf{N}_{\theta,\xi} + \mathbf{N}_{\theta,\xi}^T A_{22}\mathbf{N}_{\theta,\xi}\right)d\xi \\
& + \frac{l}{2}\int_{-1}^{1}\left(\frac{2}{l}\mathbf{N}_{w,\xi}^T - \mathbf{N}_\theta^T\right)\psi A_{33}\left(\frac{2}{l}\mathbf{N}_{w,\xi} - \mathbf{N}_\theta\right)d\xi
\end{aligned} \tag{23}$$

Similarly, the kinetic energy (13) can be written in the form

$$\mathcal{T} = \frac{1}{2}\sum_{i=1}^{ne} \dot{\mathbf{d}}_i^T \mathbf{m}_i \dot{\mathbf{d}}_i \tag{24}$$

in which

$$\mathbf{m} = \frac{l}{2}\int_{-1}^{1}\left[\left(\mathrm{N}_u^T I_{11}\mathrm{N}_u + \mathrm{N}_w^T I_{11}\mathrm{N}_w\right) - 2\mathrm{N}_u^T I_{12}\mathrm{N}_\theta + \mathrm{N}_\theta^T I_{22}\mathrm{N}_\theta\right]d\xi \tag{25}$$

are the mass matrices of the element beam.

Using the derived stiffness and mass matrices, the discretized equation of motion for the free vibration analysis of the tapered FG-CNTRC beam can be written in the form

$$\mathbf{M}\ddot{\mathbf{D}} + \mathbf{K}\mathbf{D} = \mathbf{0} \tag{26}$$

where $\mathbf{D} = \bigcup_{i=1}^{ne}\mathbf{d}_i$, $\mathbf{M} = \bigcup_{i=1}^{ne}\mathbf{m}_i$ and $\mathbf{K} = \bigcup_{i=1}^{ne}\mathbf{k}_i$ are the global nodal displacement vector, mass matrix and stiffness matrix, obtained by assembling the corresponding element vector and matrices over the total elements, respectively. For the free vibration analysis, the global nodal displacement vector **D** is assumed to be harmonic in time with circular frequency ω, and Eq. (26) becomes

$$(\mathbf{K} - \omega^2\mathbf{M})\overline{\mathbf{D}} = \mathbf{0} \tag{27}$$

with $\overline{\mathbf{D}}$ is the vector of nodal displacement amplitudes of vibration. Eq. (27) is the eigenvalue problem, which can be solved by the standard method.

5. NUMERICAL RESULTS AND DISCUSSION

Numerical investigations are presented in this section to show the accuracy of the derived beam element and to highlight the influence of various factors on the natural frequency parameters of tapered FG-CNTRC beams.

5.1. Accuracy studies

Firstly, the accuracy of the finite element model is confirmed by comparing the first frequency parameter of the FG-CNTRC beam with the results of Yas and Samadi [9], Lin and Xiang [11], respectively. To this end, two sets of the material data employed in the cited references are adopted herein as: $E_{11}^{cnt} = 600$ GPa, $E_{22}^{cnt} = 10$ GPa, $G_{12}^{cnt} = 17.2$ GPa, $E^m = 2.5$ GPa, $\nu_{12}^{cnt} = 0.19$, $\nu^m = 0.3$, $\rho^{cnt} = 1400$ kg/m^3, $\rho^m = 1190$ kg/m^3 [9]; $E_{11}^{cnt} = 5646.6$ GPa, $E_{22}^{cnt} = 7080$ GPa, $G_{12}^{cnt} = 1944.5$ GPa, $E^m = 2.5$ GPa, $\nu_{12}^{cnt} = 0.175$, $\nu^m = 0.3$, $\rho^{cnt} = 2100$ kg/m^3, $\rho^m = 1190$ kg/m^3 [11]. In addition, the CNT/matrix efficiency parameters used in the references are given in Table 1.

Table 1. CNT/matrix efficiency parameters of the FG-CNTRC beam.

V_{tcnt}	Yas and Samadi [9]			Lin and Xiang [11]		
	η_1	η_2	η_3	η_1	η_2	η_3
0.12	1.2833	1.0556	1.0556	0.137	1.022	0.715
0.17	1.3414	1.7101	1.7101	0.142	1.626	1.138
0.28	1.3238	1.7380	1.7380	0.141	1.585	1.109

Table 2 compares the fundamental frequency parameter of uniform cross-section FG-CNTRC beam of the present paper with the result of Yas and Samadi [9] for an aspect ratio L/h_0 = 15, three different values of CNT volume fraction V_{tcnt} = 0.12, 0.17, 0.28, and two different boundary conditions, namely H-H and C-H. The frequency parameter μ in Table 2 is defined according to [9] as

$$\mu = \omega L\sqrt{I_{110} / A_{110}} \tag{28}$$

with ω is the fundamental frequency of the beam and A_{110}, I_{110} is the values of A_{11}, I_{11} of a homogeneous beam made of pure matrix material, respectively. The frequency parameter for the beam obtained herein is also in good agreement with that of [9], using the generalized differential quadrature method, regardless of values of CNT volume fraction and the type of CNT distribution.

The comparison of the fundamental frequency parameter of the uniform cross-section FG-CNTRC beam obtained in the present work with that of Lin and Xiang [11] is given in Table 3 for an aspect ratio L/h_0 = 10, a total CNT volume fraction $V_{tcnt} = 0.17$ and two different boundary conditions, namely H-H and C-C. The fundamental frequency parameter $\bar{\omega}$ in Table 3 is defined as follows

$$\bar{\omega} = \omega \frac{L^2}{h_0}\sqrt{\rho^m / E_m} \tag{29}$$

where ω, as above, is the fundamental frequency of the beam. Excellent agreement between the result of the present work with that of [11] can be seen from Table 3. Noting that the first-order shear deformation theory and Ritz method have been employed in [11].

Table 2. Comparison of the fundamental frequency parameter μ of uniform FG-CNTRC beam with Yas and Samadi [9].

B.C.	Type	Source	V_{tcnt}		
			0.12	0.17	0.28
H-H	UD-CNT	Present	0.9739	1.1977	1.4348
		Ref. [9]	0.9753	1.1999	1.4401
	FGA-CNT	Present	0.9452	1.1604	1.3980
		Ref. [9]	0.9453	1.1609	1.4027
	FGO-CNT	Present	0.7521	0.9145	1.1176
		Ref. [9]	0.7527	0.9155	1.1202
	FGX-CNT	Present	1.1129	1.3795	1.6409
		Ref. [9]	1.1150	1.3830	1.6493
C-H	UD-CNT	Present	1.2412	1.5548	1.7922
		Ref. [9]	1.2444	1.5602	1.8040
	FGA-CNT	Present	1.1527	1.4334	1.6836
		Ref. [9]	1.1529	1.4344	1.6933
	FGO-CNT	Present	1.0312	1.2738	1.5153
		Ref. [9]	1.0331	1.2769	1.5229
	FGX-CNT	Present	1.3533	1.7112	1.9649
		Ref. [9]	1.3577	1.7188	1.9813

Table 3. Comparison of frequency parameter ω of uniform FG-CNTRC beam with Lin and Xiang [11].

CNT distribution	B.C.	Present	Ref. [11]
FGA-CNT	H-H	13.7208	13.7208
	C-C	17.4783	17.4782
FGX-CNT	H-H	15.3246	15.3246
	C-C	18.6043	18.6042
UD-CNT	H-H	13.9704	13.9703
	C-C	18.0081	18.0081

5.2. Effect of CNT distribution and total CNT volume fraction

The material data and the fundamental frequency parameter for all numerical calculations from this part onwards are defined according to Yas and Samadi [9] as given above. Tables 4-7 respectively list the fundamental frequency parameter μ of the H-H, C-C, C-H and C-F beams for $L/h_0 = 20$, and various values of total CNT volume fraction $V_{tcnt} = 0.12$, 0.17 and 0.28. Beams

considered herewith include uniform beam (α = 0) and tapered beams with a taper ratio α = 0.5, and all the four types of the CNT distribution, namely FGX-CNT, UD-CNT, FGA-CNT, FGO-CNT.

Table 4. Frequency parameter of H-H beam.

Type	V_{tcnt}	Uniform (α = 0)	Case A (α = 0.5)	Case B (α = 0.5)	Case C (α = 0.5)
FGX-CNT	0.12	0.9113	0.8941	0.6633	0.6212
	0.17	1.1190	1.0979	0.8075	0.7562
	0.28	1.3542	1.3286	0.9928	0.9300
UD-CNT	0.12	0.7805	0.7659	0.5575	0.5220
	0.17	0.9527	0.9348	0.6762	0.6331
	0.28	1.1601	1.1383	0.8349	0.7818
FGA-CNT	0.12	0.7533	0.7400	0.5384	0.5062
	0.17	0.9177	0.9016	0.6520	0.6130
	0.28	1.1217	1.1020	0.8058	0.7577
FGO-CNT	0.12	0.5863	0.5753	0.4095	0.3832
	0.17	0.7092	0.6959	0.4934	0.4617
	0.28	0.8746	0.8582	0.6127	0.5735

Table 5. Frequency parameter of C-C beam.

Type	V_{tcnt}	Uniform (α = 0)	Case A (α = 0.5)	Case B (α = 0.5)	Case C (α = 0.5)
FGX-CNT	0.12	1.4586	1.4308	1.2077	1.1346
	0.17	1.8467	1.8116	1.5065	1.4148
	0.28	2.1153	2.0750	1.7716	1.6649
UD-CNT	0.12	1.3415	1.3160	1.0722	1.0065
	0.17	1.6819	1.6500	1.3256	1.2440
	0.28	1.9349	1.8981	1.5702	1.4745
FGA-CNT	0.12	1.2181	1.1990	0.9551	0.9083
	0.17	1.5142	1.4908	1.1719	1.1151
	0.28	1.7811	1.7529	1.4096	1.3407
FGO-CNT	0.12	1.1180	1.0969	0.8447	0.7920
	0.17	1.3818	1.3558	1.0312	0.9666
	0.28	1.6422	1.6112	1.2516	1.1737

Table 6. Frequency parameter of C-H beam.

Type	V_{tcnt}	Uniform (α = 0)	Case A (α = 0.5)	Case B (α = 0.5)	Case C (α = 0.5)
FGX-CNT	0.12	1.1872	1.1675	0.9366	0.8801
	0.17	1.4845	1.4601	1.1556	1.0856
	0.28	1.7384	1.7094	1.3861	1.3028
UD-CNT	0.12	1.0601	1.0428	0.8110	0.7616
	0.17	1.3137	1.2925	0.9937	0.9329
	0.28	1.5487	1.5232	1.2001	1.1272
FGA-CNT	0.12	0.9591	0.9457	0.7239	0.6880
	0.17	1.1795	1.1633	0.8815	0.8381
	0.28	1.4141	1.3942	1.0752	1.0219
FGO-CNT	0.12	0.8428	0.8295	0.6175	0.5794
	0.17	1.0309	1.0147	0.7489	0.7026
	0.28	1.2471	1.2273	0.9195	0.8629

Table 7. Frequency parameter of C-F beam.

Type	V_{tcnt}	Uniform (α = 0)	Case A (α = 0.5)	Case B (α = 0.5)	Case C (α = 0.5)
FGX-CNT	0.12	0.3480	0.3438	0.2484	0.2337
	0.17	0.4237	0.4186	0.3009	0.2831
	0.28	0.5209	0.5146	0.3734	0.3513
UD-CNT	0.12	0.2925	0.2890	0.2065	0.1943
	0.17	0.3547	0.3506	0.2497	0.2348
	0.28	0.4380	0.4328	0.3106	0.2909
FGA-CNT	0.12	0.2456	0.2438	0.1752	0.1678
	0.17	0.2962	0.2941	0.2108	0.2020
	0.28	0.3668	0.3642	0.2622	0.2513
FGO-CNT	0.12	0.2148	0.2123	0.1499	0.1410
	0.17	0.2588	0.2558	0.1802	0.1695
	0.28	0.3214	0.3177	0.2246	0.2113

It is observed from the results in Tables 4 to 7 that the frequency parameter of the beam increases with increasing the total CNT volume fraction V_{tcnt}, regardless of the taper case, the

type of CNT distribution and the boundary condition. Among the four types of the CNT distribution, the FGX-CNT beam has the highest frequency parameters while the FGO-CNT beam has the lowest one, and sequential order of the frequency parameter is as follow: $\mu_{\text{FGX-CNT}} > \mu_{\text{UD-CNT}} > \mu_{\text{FGA-CNT}} > \mu_{\text{FGO-CNT}}$. Additionally, the effect of the four boundary conditions on the fundamental frequency parameter is also seen as such that the highest frequencies are obtained for the C-C beams, followed by C-H and H-H beams, and the C-F beam has the lowest fundamental frequency parameter at every total CNT volume fraction and CNT distribution type, $\mu_{\text{C-C}} > \mu_{\text{C-H}} > \mu_{\text{H-H}} > \mu_{\text{C-F}}$. Comparing the uniform beam, the tapered beams, as seen from the tables, have lower frequencies, and among the three taper cases, the case C beam has the lowest frequencies, regardless of the boundary condition.

The effect of the total CNT volume fraction on the frequency parameter is shown in Table 8, where the changes on the frequency parameter by increasing the total CNT volume fraction are given for the C-C beam. The data in Table 8 are obtained based on the frequency parameters of Table 5, and they are calculated, for example, when V_{tcnt} increases from 0.12 to 0.17 as $\frac{\left|\mu_{0.12}-\mu_{0.17}\right|}{\left|\mu_{0.12}\right|}100\%$. It can be seen from Table 8 that the increase of the frequency parameter by increasing the total CNT volume fraction is almost the same for the uniform beam and the case A tapered beam, regardless of the CNT distribution type. The effect of the total CNTs volume fraction on the frequency parameter of the tapered beams with case B and case C is less significant than that of the uniform beam and the case A tapered beam when V_{tcnt} increases from 0.12 to 0.17. On the other hand, this influence of the case B and case C tapered beams is more significantly compares to that of the uniform and case A tapered beams when V_{tcnt} increases from 0.17 to 0.28. In other words, the effect of the total CNT volume fraction on the fundamental frequency depends on the taper case of the tapered FG-CNTRC beams.

Table 8. The change on frequency parameter by increasing total CNT volume fraction V_{tcnt} of C-C beams.

Type	V_{tcnt} increase	Uniform (%)	Case A (%)	Case B (%)	Case C (%)
FGX-CNT	$0.12 \rightarrow 0.17$	26.61	26.61	24.74	24.70
	$0.17 \rightarrow 0.28$	14.54	14.54	17.60	17.68
UD-CNT	$0.12 \rightarrow 0.17$	25.37	25.38	23.63	23.60
	$0.17 \rightarrow 0.28$	15.04	15.04	18.45	18.53
FGA-CNT	$0.12 \rightarrow 0.17$	24.31	24.34	22.70	22.77
	$0.17 \rightarrow 0.28$	17.63	17.58	20.28	20.23
FGO-CNT	$0.12 \rightarrow 0.17$	23.60	23.60	22.08	22.05
	$0.17 \rightarrow 0.28$	18.84	18.84	21.37	21.43

5.3. Effect of taper ratio and aspect ratio

The taper ratio α versus frequency parameter μ of the FG-CNTRC beam with three boundary condition, H-H, C-C and C-F is shown in Figs. 4-6, respectively. The figures are illustrated for the beam with an aspect ratio $L/h_0 = 20$, a total CNT volume fraction $V_{tcnt} = 0.28$.

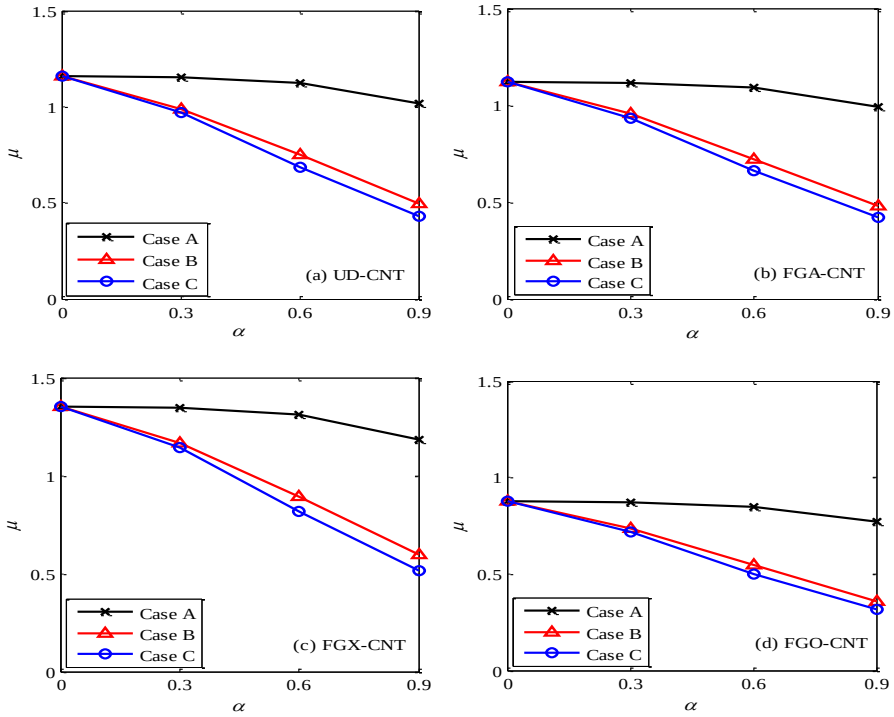

Figure 4. Taper ratio versus frequency parameter of H-H beam with V_{tcnt} = 0.28, L/h_0 = 20 and different types of CNT distribution.

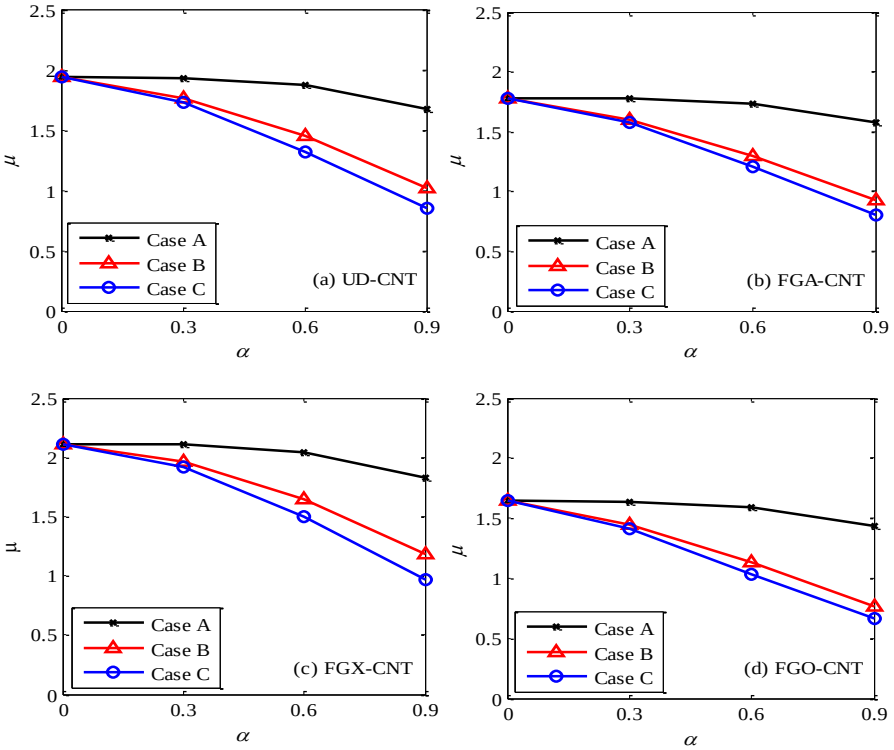

Figure 5. Taper ratio versus frequency parameter of C-C beam with V_{tcnt} = 0.28, L/h_0 = 20 and different types of CNT distribution.

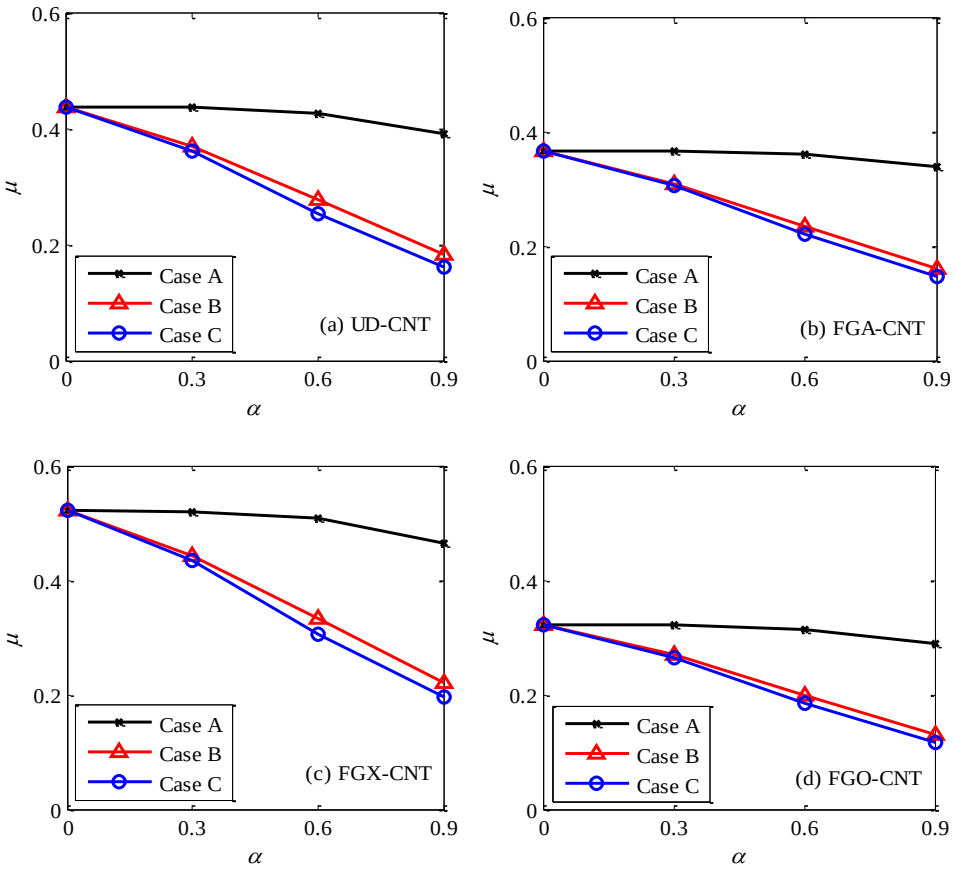

Figure 6. Taper ratio versus frequency parameter of C-F beam with Vtcnt = 0.28, L/h0 = 20 and different types of CNT distribution.

One can see from the figures that the variation of the frequency parameter with the taper ratio much depends on the taper case, regardless of the boundary condition. For all the three boundary conditions, the frequency parameter decreases by the increase of the taper ratio, irrespective of the CNT distribution type. The decrease of the frequency by increasing the taper ratio, as seen from the figures, is the most significant for the type C tapered beam, while that is the least for the type A tapered beam. The type of CNT distribution also plays an important role in the variation of the frequency parameter with the taper ratio, and the variation rate of the parameter μ with taper ratio α of the UD-CNT and FGX-CNT beams is more significant than that of the FGA-CNT and FGO-CNT beams.

The frequency parameters of the H-H beams with a total CNT fraction V_{tcnt} = 0.17 and different values of the aspect ratio L/h_0 are given in Tables 9 and 10 for two types of CNT distribution, namely UD-CNT and FGX-CNT, respectively. The effects of the aspect ratio on the frequency parameter are clearly seen from the tables. The frequency parameter of the FG-CNTRC beam steadily deceases when increasing the aspect ratio, and this tendency is correct for both the uniform and tapered beams. Besides, the decrease of the frequency parameter of the tapered beam is more significant compares to that of the uniform beam, and this tendency is correct for both the two types of the CNT distribution considered herewith. By comparing the

frequency parameter in Table 9 and 10 one can see that the influence of the aspect ratio on the frequency parameter of the UD-CNT beam is more significant on that of the FGX-CNT beam.

Table 9. Frequency parameter of UD-CNT beam with different aspect ratios L/h_0.

L/h_0	Uniform ($\alpha = 0$)	Case A ($\alpha = 0.5$)	Case B ($\alpha = 0.5$)	Case C ($\alpha = 0.5$)
5	2.0677	2.0281	1.7995	1.6925
10	1.5659	1.5362	1.2082	1.1330
15	1.1977	1.1752	0.8734	0.8181
20	0.9527	0.9348	0.6762	0.6331
25	0.7852	0.7705	0.5494	0.5142
30	0.6656	0.6531	0.4618	0.4321
35	0.5765	0.5657	0.3979	0.3723
40	0.5080	0.4985	0.3494	0.3269

Table 10. Frequency parameter of FGX-CNT beam with different aspect ratios L/h_0.

L/h_0	Uniform ($\alpha = 0$)	Case A ($\alpha = 0.5$)	Case B ($\alpha = 0.5$)	Case C ($\alpha = 0.5$)
5	2.1681	2.1265	1.9410	1.8271
10	1.7404	1.7073	1.3875	1.3021
15	1.3795	1.3535	1.0303	0.9655
20	1.1190	1.0979	0.8075	0.7562
25	0.9326	0.9151	0.6603	0.6181
30	0.7958	0.7809	0.5570	0.5213
35	0.6924	0.6794	0.4810	0.4502
40	0.6118	0.6004	0.4230	0.3958

6. CONCLUSIONS

In this paper, the free vibration of tapered FG-CNTRC beams has been studied by a finite element model. The beams with four types of CNT distribution are considered to be linearly tapered in longitudinal direction by three different cases. Based on the first-order shear deformation theory, equations of motion with variable coefficients of the beams are derived from Hamilton principle. A two-node beam element using hierarchical functions to interpolate the displacement field was formulated and employed to compute the frequency of the beams. The numerical results reveal that CNT distribution and the taper ratio play an important role on the vibration frequencies. Among the four types of the CNT distribution considered herein, the FGX-CNT gives the highest frequencies, while the FGO-CNT results in the lowest ones. It has been shown that the taper case plays an important role on the influence of the total CNT volume

fraction on the frequencies of the beams, and the dependence of the frequency parameter upon the aspect ratio of the FG-CNTRC tapered beam is also influenced by the tapered case. A parametric study has been carried out to illustrate the effects of other factors, including the total CNT volume fraction, the taper ratio, taper case and the aspect ratio on the frequency parameter of the beams are also examined and highlighted.

REFERENCES

1. Li Y., Wang K., Wei J., Gu Z., Wang Z., Luo J. and Wu D. - Tensile properties of long aligned double-walled carbon nanotubes strands, Carbon **43** (2005) 31-35.
2. Qin Z., Qin Q. H. and Feng X. Q. - Mechanical property of carbon nanotubes with intramolecular junctions: molecular dynamics simulations, Phys. Lett. A **372** (44) (2008) 6661-6666.
3. Fiedler B., Gojny F. H., Wichmann M. H. G., Nolte M. C. M. and Schulte K. - Fundamental aspects of nano-reinforced composites, Compos Sci Technol. **66** (16) (2006) 3115-3125.
4. Esawi A. M. K. and Farag M. M. - Carbon nanotube reinforced composites: potential and current challenges, Mater. Des. **28** (2007) 2394-2401.
5. Rajoria H. and Jalili N. - Passive vibration damping enhancement using carbon nanotube-epoxy reinforced composite, Compos. Sci. Technol. **65** (14) (2005) 2079-2093.
6. Zhou X., Shin E., Wang K. W., and Bakis C. E. - Interfacial damping characteristics of carbon nanotube-based composites, Compos. Sci. Technol. **64** (15) (2004) 2425-2437.
7. Ma P. C. and Kim J. K. - Carbon nanotubes for polymer reinforcement, CRC Press, Boca Raton (2011).
8. Ke L. L., Jang J. and Kitipornchai, S. - Nonlinear free vibration of functionally graded carbon nanotube-reinforced composite beams, Compos. Struct. **92**(3) (2010) 676-683.
9. Yas M.H. and Samadi N. - Free vibrations and buckling analysis of carbon nanotube-reinforced composite Timoshenko beams on elastic foundation, Int. J. Pres. Vessels and Pip. **98** (2012) 119-128.
10. Shen H. S. - Nonlinear bending of functionally graded carbon nanotube reinforced composite plates in thermal environments, Compos. Struct. **91** (2009) 9-19.
11. Lin F., and Xiang Y. - Vibration of carbon nanotube reinforced composite beams based on the first and third order beam theories, App. Math. Model. **38** (2014) 3741-3754.
12. Wattanasakulpong N. and Ungbhakorn V. - Analytical solutions for bending, buckling and vibration responses of carbon nanotube-reinforced composite beams resting on elastic foundation, Comp. Mater. Sci. **71** (2013) 201-208.
13. Nejati M., Eslampanah A. and Najafizadeh M. - Buckling and vibration analysis of functionally graded carbon nanotube-reinforced beam under axial load, Int. J. Appl. Mech. **8**(1) (2016) 1650008. https://doi.org/10.1142/S1758825116500083
14. Wu H. L., Yang J. and Kitipornchai S. - Nonlinear vibration of functionally graded carbon nanotube-reinforced composite beams with geometric imperfections, Compos. Part B: Eng. **90** (2016) 86-96.

15. Wu H. L., Yang J. and Kitipornchai S. - Imperfection sensitivity of thermal post-buckling behaviour of functionally graded carbon nanotube-reinforced composite beams, App. Math. Model. **42** (2017) 735-752.
16. Wu H. L., Kitipornchai S., and Yang J. - Free vibration of thermo-electro-mechanically postbuckled FG-CNTRC beams with geometric imperfections, Steel Compos. Struct. **29**(3) (2018) 319-332.
17. Shahba A., Attarnejad R., Marvi M. T. and Hajilar S. - Free vibration and stability analysis of axially functionally graded tapered Timoshenko beams with classical and non-classical boundary conditions, Compos. Part B: Eng. **42** (2011) 801-808.
18. Gan B. S., Trinh T. H., Le T. H. and Nguyen D. K. - Dynamic response of non-uniform Timoshenko beams made of axially FGM subjected to multiple moving point loads, Struct. Eng. Mech. **53** (2015) 981-995.
19. Nguyen D. K. - Large displacement response of tapered cantilever beams made of axially functionally graded material, Compos. Part B: Eng. **55** (2013) 298-305.
20. Nguyen D. K. - Large displacement behaviour of tapered cantilever Euler–Bernoulli beams made of functionally graded material, App. Math. Comput. **237** (2014) 340-355.
21. Nguyen D. K. and Gan B. S. - Large deflections of tapered functionally graded beams subjected to end forces, App. Math. Model. **38** (2014) 3054-3066.
22. Nguyen D. K. and Tran T. T. - Free vibration of tapered functionally graded beams using an efficient shear deformable finite element model, Steel Compos. Struct. **29**(3) (2018) 363-377.
23. Akin J. E. - Finite elements for analysis and design, Academic Press, London, 1994.
24. Zienkiewicz O. C., and Taylor R. L. - The Finite Element Method, 4th edition, Mc. Graw-Hill Book Company, London, 1997.
25. Cook R. D., Malkus D. S., and Plesha M. E. - Concepts and applications of finite element analysis, 3rd edition, John Willey & Sons, New York, 1989.